Nano Energy 49 (2018) 51–58

Contents lists available at ScienceDirect

Nano Energy

journal homepage: www.elsevier.com/locate/nanoen

Full paper

Hybrid generator based on freestanding magnet as all-direction in-plane energy harvester and vibration sensor

Xuexian Chen[a,b], Hang Guo[a,b], Hanxiang Wu[a], Haotian Chen[a,b], Yu Song[a], Zongming Su[a], Haixia Zhang[a,b,*]

[a] National Key Lab of Micro/Nano Fabrication Technology, Peking University, Beijing 100871, China
[b] Academy for Advanced Interdisciplinary Studies, Peking University, Beijing 100871, China

ARTICLE INFO

Keywords:
Triboelectric
Electromagnetic
Vibration sensor
Energy harvesting

ABSTRACT

Vibration is a widely existing mechanical phenomenon containing enormous energy that can be transformed into electricity without polluting the environment. However, most current mechanical energy harvesters only can scavenge energy from a specific direction, resulting in the waste of energy from other directions. Here, we propose a triboelectric-electromagnetic hybrid generator built on freestanding magnet (FMHG), which is able to harvest low-frequency vibration energy from arbitrary in-plane directions. Besides, it can detect vibration direction from periodical or pulse movement. Under the excitation of shaker, maximum power of 85.7 μW and 3.29 mW are obtained by one electrode pair of the TENG and EMG respectively, which can charge a capacitor of 20 μF to 7 V rapidly benefiting from the hybrid configuration. The hybrid generator can light up commercial LEDs driven by human running and bicycle braking, as well as distinguish leg movement in eight directions, proving its application potential in building up self-powered sensing systems such as alarms, environmental monitor and human-machine interface.

1. Introduction

Harvesting energy from ambient environment is of significant importance for realizing self-powered systems and meeting rapidly increasing energy demands. Vibration is a common mechanical motion form that is widely existing in our ambient environment, such as the body movement, swaying of trees, slight wobble of buildings, and ocean wave oscillations [1–5]. It can be converted into electricity through various mechanisms *i.e.* electrostatics [6,7], electromagnetic [8,9], and piezoelectric effects [10–13]. Moreover, by coupling triboelectric effect and electrostatic induction, triboelectric nanogenerator (TENG) has been successfully developed to scavenge low-frequency mechanical energy in ambient environment [14–22]. Furthermore, to acquire a higher energy conversion efficiency and broaden the operating bandwidth, hybridization of TENG and electromagnetic generator (EMG) has been demonstrated due to the high output of EMG in high frequency range. For example, the hybridized nanogenerator for efficiently scavenging of biomechanical energy based on contact-separation mode TENG [23], the waterproof hybrid nanogenerator for harvesting water wave or flow energy built on rotary TENG [24,25], and the hybridization of sliding-mode TENG and EMG for high-efficient mechanical energy harvesting [26]. However, a vibration energy harvester that can scavenge energy from multiple directions is highly demanded since the vibration in realistic environment is random and varying [27,28].

Except for energy conversion, vibration is a useful media for providing messages of external motion since it contains plenty of characteristics like direction, amplitude and frequency [29,30]. However, commercially available vibration sensors cannot detect the motion direction and always need a power source to realize their function. To build up self-powered sensing systems, TENG is a powerful tool that has been applied in various self-powered sensors, such as angle detection [31,32], acceleration sensing [33,34], tactile mapping [35,36], environmental testing [37,38] and healthcare monitoring [39–41], *etc*.

Herein, we presented a newly designed FMHG based on triboelectric and electromagnetic mechanisms for scavenging low-frequency vibration energy and detecting multi-directional in-plane vibration actively. The TENG part can work effectively over a wide frequency range and detect vibration direction based on the eight-petal electrodes (four electrode pairs). At the same time, the EMG part can achieve much higher power output under large displacement. Under the excitation of 12 Hz, maximum output power of 85.7 μW and 3.29 mW were achieved by one electrode pair of TENG and EMG, respectively. Benefiting from the hybridization configuration, the device can charge a capacitor of 20 μF to 7 V in 200 s, which is superior to TENG only (4.5 V) and EMG

* Corresponding author at: National Key Lab of Micro/Nano Fabrication Technology, Peking University, Beijing 100871, China.
E-mail address: zhang-alice@pku.edu.cn (H. Zhang).

https://doi.org/10.1016/j.nanoen.2018.04.024
Received 13 January 2018; Received in revised form 31 March 2018; Accepted 9 April 2018
Available online 13 April 2018

only (1.2 V). To show its powerful ability of energy harvesting, the device is used to collect low-frequency vibration energy like human running and bicycle brake, which is strong enough to light up 40 LEDs. As a demonstration of direction detection, we utilize the hybrid generator to recognize motion of leg in eight directions, where the device can work as a human-machine interface to play a game, showing its potential in self-powered sensing systems, such as the environmental monitor, security equipment and motion sensors.

2. Experiment

2.1. Fabrication of the hybrid generator

Firstly, two acrylic sheets with dimensions of $\Phi = 100\,mm \times 2\,mm$ (diameter × thickness) prepared by laser cutting were used as bottom substrate and top cover. An acrylic circular side wall with outer diameter of 100 mm, thickness of 2 mm and height of 10 mm was fabricated with the same method. Two magnets with the size of $\Phi = 30\,mm \times 2\,mm$ are bonded together as a mass and suspended by four springs attached to the bottom substrate. The spring has a wire diameter of 0.3 mm, a free length of 20 mm and outer diameter of 3 mm. The eight-petal electrode and coil were fabricated through the same FPCB technique, that was depositing a layer of copper on the Kapton substrate, then getting the designed pattern through photolithography process and finally laminating another layer of Kapton on the top. The eight-petal electrode has a diameter of 60 mm and a gap of 1 mm between each part. The coil has 10 layers and each layer has an outer diameter, wire width and gap width of 60 mm, 0.254 mm and 0.254 mm, respectively. Then, the electrode and coil film are respectively adhered to the substrate and cover, which are bonded together with the side wall.

2.2. Measurement system

The hybrid generator is anchored on the electrodynamic shaker to test the output performance of the device under different excitations. The output current of the device was measured by a low-noise current preamplifier (Stanford Research SR570) and all the signals were recorded and displayed through a digital oscilloscope (Agilent DSO-X 2014A).

3. Design and analysis

The basic unit of the hybrid generator is schematically presented in Fig. 1a, which has a discoid structure with circular acrylic as support shell. The EMG consists of a copper coil lying at the center of the top cover. At the center of the discoid shell, a special strong magnet with a diameter of 3 cm is mobile and suspended by four identical springs with an included angle of 90° between each other, which can provide a magnetic field and act as an oscillator. The TENG is composed of a thin Aluminum film covered on the surface of magnet as a metal friction layer during vibration (Fig. 1b). A Kapton thin film attached to the bottom substrate works as the dielectric friction layer with deposited copper as the back electrode, which has an eight-petal shape as shown in Fig. 1c. The designed structure of the electrode enables that the whole system can detect vibration and harvest energy in arbitrary in-plane directions since every two electrodes in opposite (denoted as *En* and *En'* (n = 1,2,3,4), respectively) together with the dielectric and metal friction layers can form a freestanding TENG. Fig. 1d,e display the photographs of the fully packaged hybrid generator and its inner structure, respectively. The detailed fabrication process is described in the Experimental section.

3.1. Working principle

According to previous report, the vibration energy harvester can be simplified as a second-order spring-mass-damper system with the forced vibration along single direction [21,38]. The simplified sliding model and corresponding analysis are shown in Supporting information Fig. S1. The working mechanism of the FMHG in half cycle is schematically depicted in Fig. 2a, where the electricity generation consists of two parts: one is from the freestanding TENG and the other is from the EMG. Due to the higher electron affinity of Kapton than that of Aluminum, the surface of Kapton film is covered with negative triboelectric charges while the Aluminum surface is covered by positive triboelectric charges. At original position, the magnet locates at the center of the Kapton film, inducting equal negative charges on each electrodes under the overlap area (Fig. 2a, stage I). Once the device moves along arbitrary in-plane direction, a displacement will be established between the magnet and the substrate. Therefore, the inductive potential of the electrode pair along motion direction becomes different, driving free electrons on the leaving electrode to the forward electrode and generating triboelectric current in backward direction. At the same time, the magnetic flux crossing the copper coil increases and clockwise current can be generated at the coil according to the Lenz's law. This process is shown in Fig. 2a, stage II. The flow of the inductive electrons and EMG current last until the relative displacement reaches the maximum (Fig. 2a, stage III). Subsequently, as the displacement is

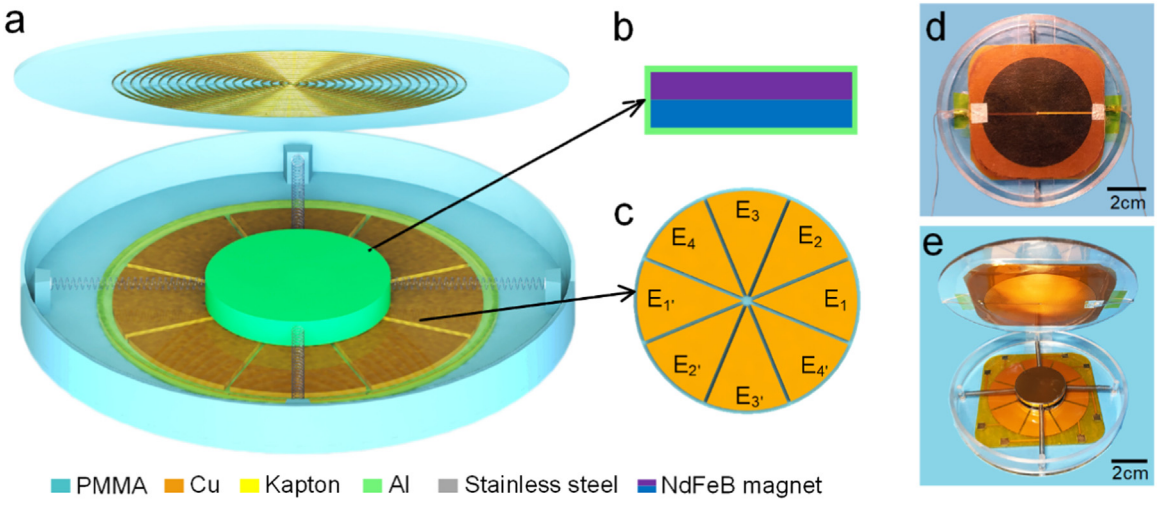

Fig. 1. Structure design of the hybrid generator. (a) Schematic illustration of the device. (b) Inner structure of the mass. (c) Structure design of the eight-petal electrode. (d) Photograph of the hybrid generator after assembling. (e) Photograph of the device before assembling.

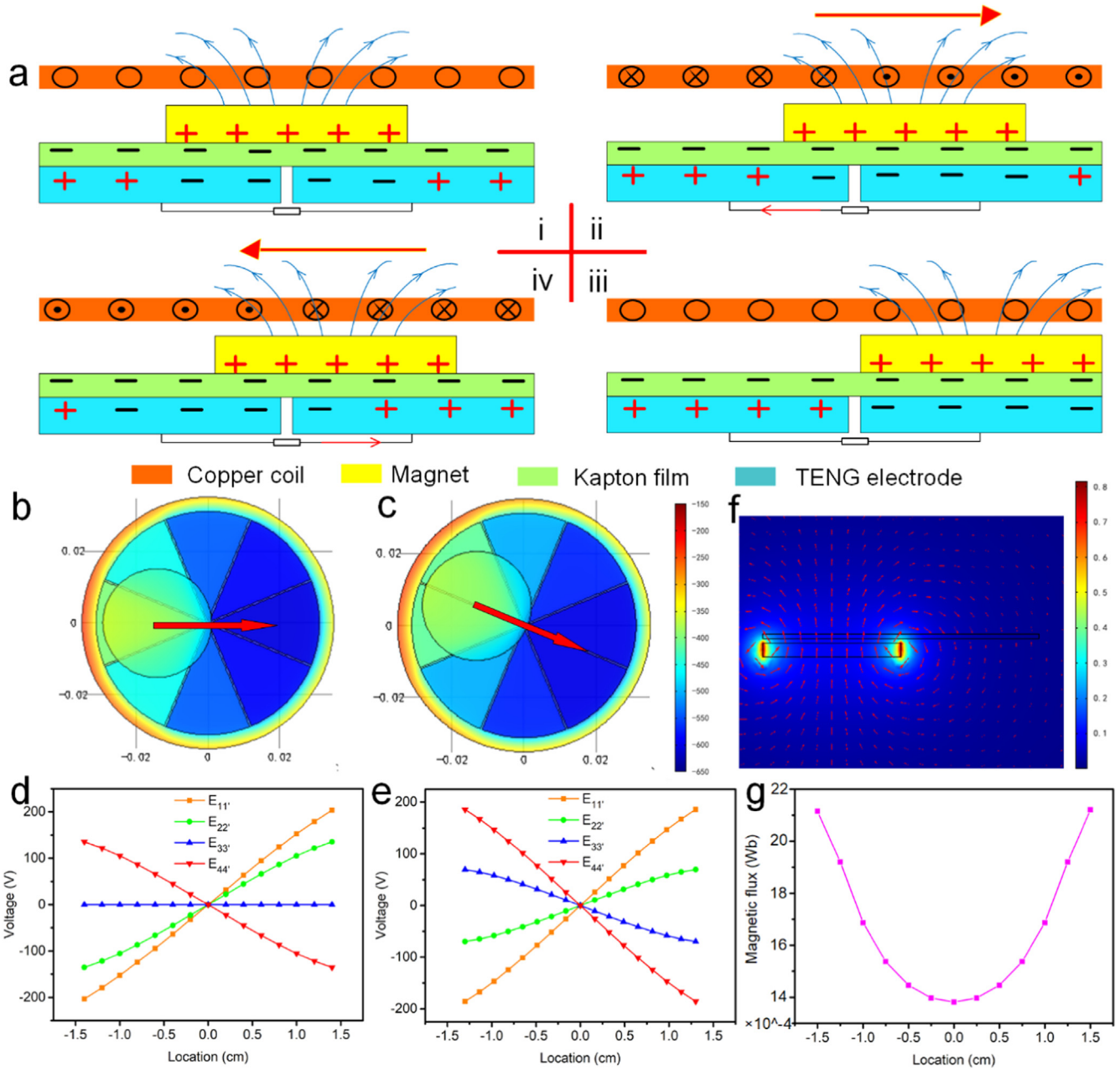

Fig. 2. Working mechanism of the hybrid generator. (a) Schematic diagram showing the power generation process of the device in half cycle. Numerical analysis of the potential distribution across the TENG electrode when the mass moves along (b) the direction of 11′ and (c) the direction between 11′ and 44′. Simulated output of four electrode pairs when the mass moves across the electrode along (d) the direction of 11′ and (e) the direction between 11′ and 44′. (f) Simulated magnetic field distribution of the EMG. (g) The simulated magnetic flux over the coil in the perpendicular direction when magnet locates at different position.

decreased by the spring force, the potential difference between the electrode pair becomes smaller and the inductive electrons flow back to the leaving electrode, forming a forward triboelectric current. Meanwhile, the magnetic flux crossing the copper coil decreases, generating a anticlockwise EMG current (Fig. 2a, stage IV). Then the magnet reverts to the initial state and repeats the process on the other side. In brief, when the magnet moves to the edge of the device, the TENG current will flow from the forward electrode to the leaving electrode and the current direction in the coil is clockwise. In the contrast, when the magnet moves back to the center, the current direction in the TENG is also from the forward electrode to the leaving electrode while that for the EMG is anticlockwise.

Finite element analysis was employed to calculate the potential distribution of TENG and the magnetic field distribution of EMG. The results of TENG when the magnet moves across the electrode are displayed in Fig. 2b, c. In the simulation, the surface charge density of the Kapton film and Aluminum film were set as $-10\ \mu C/m^2$ and $10\ \mu C/m^2$, respectively. According to previous study, assuming that the surface charge density on the Kapton is uniform, the open-circuit voltage of TENG can be expressed as [42]

$$V_{oc} = \frac{Q_{sc}}{C} = \frac{\Delta S \cdot \sigma}{C} \quad (1)$$

where Q_{sc} is the transferred charge in the short-circuit, C is the capacitance between two electrodes and σ is the surface charge density on the magnet. Since the transferred charge is induced by the triboelectric charge on the magnet, the value of the potential difference for the four pairs of electrode is positive related to the changes of contact area (ΔS). When the mass moving to a certain direction, the electrode along the

direction has the maximum area changes and thus generating highest output. Fig. 2d and e present the potential difference of the four electrode pairs when the mass moves along the direction of 11′ and the direction between 11′ and 44′, respectively. Therefore, by comparing output from the four pairs of electrodes, the vibration direction can be easily determined.

The magnetic field distribution of EMG is shown in Fig. 2f and the magnetic flux ϕ across the coil in perpendicular direction are shown in Fig. 2g when the mass locates at different places. According to Faraday law of electromagnetic induction, the output of the coil can be calculated as

$$\varepsilon(t) = -n\frac{d\phi}{dt} = -nA\frac{dB}{dz}\frac{dz}{dt} \quad (2)$$

where, ε is the induced electromotive force, n is the turns of coil, A is the area of the coil, $\frac{dB}{dz}$ is the change rate of magnetic flux intensity with position and $\frac{dz}{dt}$ is the velocity of the magnetic. From Eq. (2), by increasing either the number of coils or the moving displacement of the magnet, the amplitude of $\varepsilon(t)$ increase. As can be seen from the simulation results, the magnetic field intensity at the edge of the magnet is much larger than other area and the gradient of magnetic flux increases as the magnet moves off the center. Therefore, a nonlinear growth of output can be obtained when the displacement of magnet increases. Meanwhile, the magnet can be designed to an array structure to further improve the magnetic flux intensity. From the Eqs. (1) and (2) can be seen, when the magnet has a relative displacement to the substrate, both the contact area and the magnetic flux in the coil will change, thus generating both triboelectric and electromagnetic output.

We also investigate the influence of the mass with radius varies from 0.5 cm to 2.5 cm on the output of the device through simulation. The potential distribution of the TENG and magnetic field distribution of EMG when the mass is small and large are presented in Fig. S2. The largest output of TENG appears on the radius ranges from 1.5 cm to 1.7 cm while the magnetic flux changes of EMG maintain at a relative high level with the radius ranges from 0.5 cm to 1.5 cm. Considering the above factors, we design the magnet with a radius of 1.5 cm.

4. Results and discussion

To characterize the performance of the hybrid generator, electrical output measurement was carried out under periodical movement of 12 Hz generated by a shaker. The magnet will reciprocate along the driving direction and generate periodical signal at the four pairs of electrode and the coil, as shown in Fig. 3a. The output voltage and short-circuit current of TENG part after 50 Hz digital filter are shown in Fig. 3b and c respectively, under the motion direction of 11′. The further signal process of the output can reduce the influence of noise and make it easier to distinguish the vibration direction. As expected in the working principle section, the electrode pair along the motion direction ($E_{11'}$) have the largest output while that perpendicular the motion direction ($E_{33'}$) have the smallest output and the output for electrodes at the diagonal direction ($E_{22'}$ and $E_{44'}$) lies between them. Numerically,

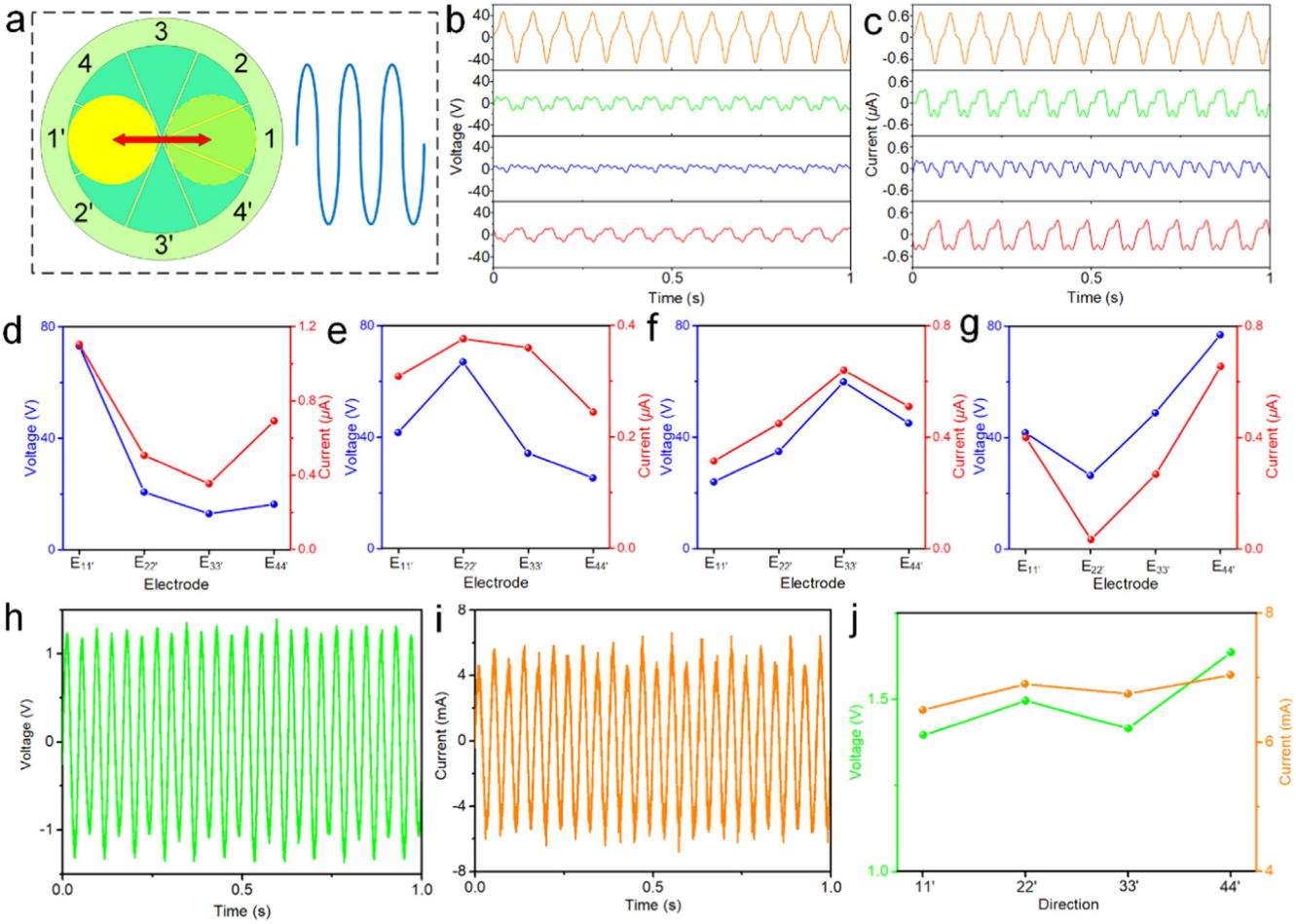

Fig. 3. Output performance of the device under periodical excitation. (a) Schematic illustration showing the motion of mass under a sinusoidal signal. (b) Output voltage and (c) short-circuit current waveforms of the four electrode pairs of TENG under the motion direction of 11′. (d-g) The comparison of maximum output voltage and current of the TENG electrodes under the motion direction of 11′, 22′, 33′ and 44′, respectively. (h) Output voltage and (i) current of the EMG under the motion direction of 11′. (j) The output comparison of EMG with the device moving along four directions.

the maximum voltages for the electrodes $E_{11'}$ to $E_{44'}$ are 73.1 V, 41.6 V, 23.9 V and 41.8 V, respectively, and the short-circuit currents are 1.10 μA, 0.51 μA, 0.35 μA and 0.69 μA, respectively. The output waveforms for the four pairs of electrode along three other directions are shown in the Fig. S3, which presents the same characteristics as the direction of 11′. It should be noted that the friction surface charge on the Kapton layer in measurement is not as uniform as the simulation, which will cause output on the electrode perpendicular to the motion direction and the inequality for the two electrode pairs at the diagonal direction. Fig. 3d to g show the comparisons of output voltage and current among the four pair of electrodes when the device is excited along the direction of 11′, 22′, 33′ and 44′, respectively. Obviously, both the output voltage and current are the largest for the pair of electrodes along the motion direction. The output performance of the EMG part is also investigated at the same time. Fig. 3h, i show the output voltage and current waveforms of the EMG along the direction of 11′, where the maximum output voltage and current are 1.39 V and 6.5 mA, respectively. The comparison of the output voltage and current of EMG at four vibration directions is shown in Fig. 3j, which shows little discrepancy.

As a resonate device, the frequency response of the FMHG is investigated by employing an electrodynamic shaker to provide sinusoidal output with a range of vibration frequency from 5 Hz to 50 Hz. The results of TENG part are shown in Fig. S4, which prove that the TENG is capable of harvesting vibration energy from all of the in-plane directions with a wide working bandwidth of 10 Hz in low-frequency range. When vibrating along the direction of 11′ and 33′, the system resonates at the frequency of 15 Hz and the maximum output voltages of 85.2 V and 84.2 V can be obtained at the electrode of $E_{11'}$ and $E_{33'}$, respectively. When it comes to the vibration direction of 22′ and 44′, the resonate frequency is 14 Hz and the largest output voltage at corresponding electrodes are 106.9 V and 124.3 V, respectively. Based on above analysis, the magnet has the largest displacement when the vibration frequency is near the resonant frequency, which will make the magnet beyond the area of electrode. For the directions of 11′ and 33′, the maximum displacement of the magnet is confined by the spring, which has an incompressible original length. While for the directions of 22′ and 44′, the boundary of movement is the acrylic shell. Therefore, the larger displacement at the directions of 22′ and 44′ will cause a higher output than that of 11′ and 33′. Notably, in the four directions, the electrode pair at the vibration direction has the largest output over a wide range of frequency. The frequency responses of the EMG at different directions are shown in Fig. S5, which present much smaller bandwidth compared to the TENG part. The maximum output voltages of EMG at four directions (from 11′ to 44′) are 1.39 V, 1.49 V, 1.41 V and 1.64 V, respectively, while the maximum currents are 6.5 mA, 6.9 mA, 6.7 mA and 7.0 mA, respectively.

To evaluate the output capability of the device, the maximum output power of TENG part and EMG part when connected to different external load resistance were measured and calculated. For the TENG part, the electric output is mainly contributed by the electrode pair along the vibration direction. As illustrated in Fig. 4a, instantaneous peak power of 72.5 μW @ 400 MΩ, 83.9 μW @ 400 MΩ, 65.5 μW @ 500 MΩ and 85.7 μW @ 600 MΩ are achieved by the four electrode pairs when the device vibrates along the direction of 11′, 22′, 33′ and 44′, respectively. When it comes to the EMG part, the maximum values are 1.65 mW, 2.89 mW, 1.65 mW and 3.29 mW at the matched load of 280 Ω for the four directions, respectively (Fig. 4b). In accordance with the preceding measurement result, the displacement of magnet is larger at the direction of 22′ and 44′ than the others under the same excitation. Consequently, higher instantaneous peak power was obtained at these directions for both the TENG and EMG part. The impedance matching between TENG and EMG can be achieved through transformers [43]. Furthermore, the output of the hybrid generator was demonstrated to charge a 20 μF capacitor through rectifier. The corresponding circuit diagram is illustrated in Fig. 4c. The charging voltage curves of the capacitor using TENG only, EMG only and hybrid generator are plotted in Fig. 4d, which proves the benefit of hybridization configuration. Although the EMG has a larger output power and current, which can charge the capacitor quickly to 1.2 V, the property of low output voltage limits its final charging level. Due to the high output voltage but low output current of TENG, the capacitor can be charged to

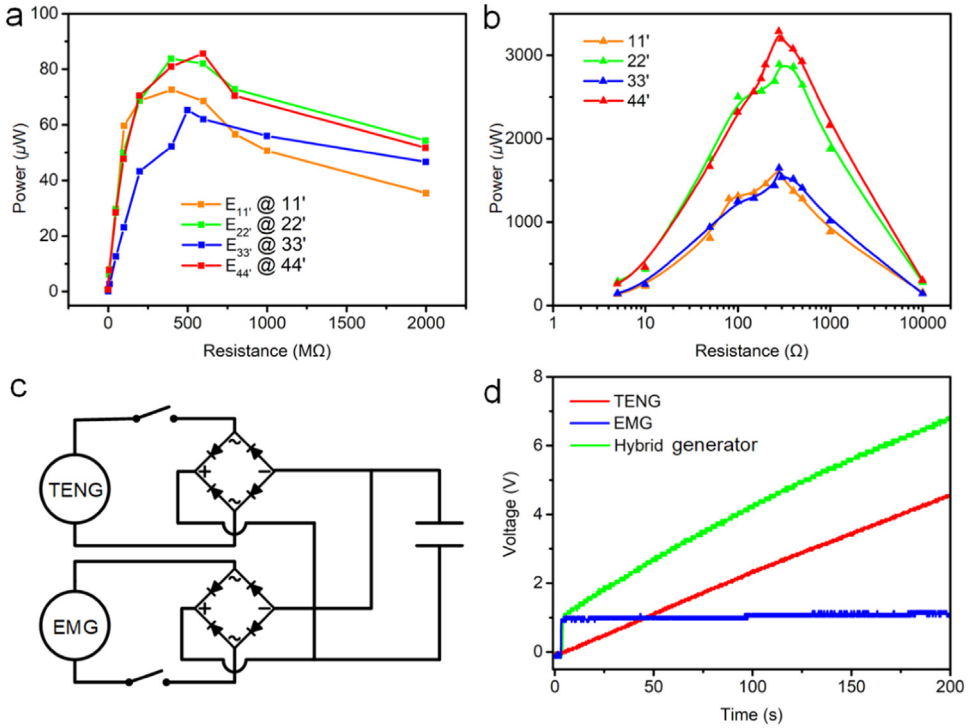

Fig. 4. Output power performances of TENG and EMG. Dependence of output power on the load resistance along four directions of (a) the TENG and (b) the EMG. (c) Circuit diagram for charging capacitors by the hybrid device. (d) Charging curves of a 20 μF capacitor using the hybrid generator.

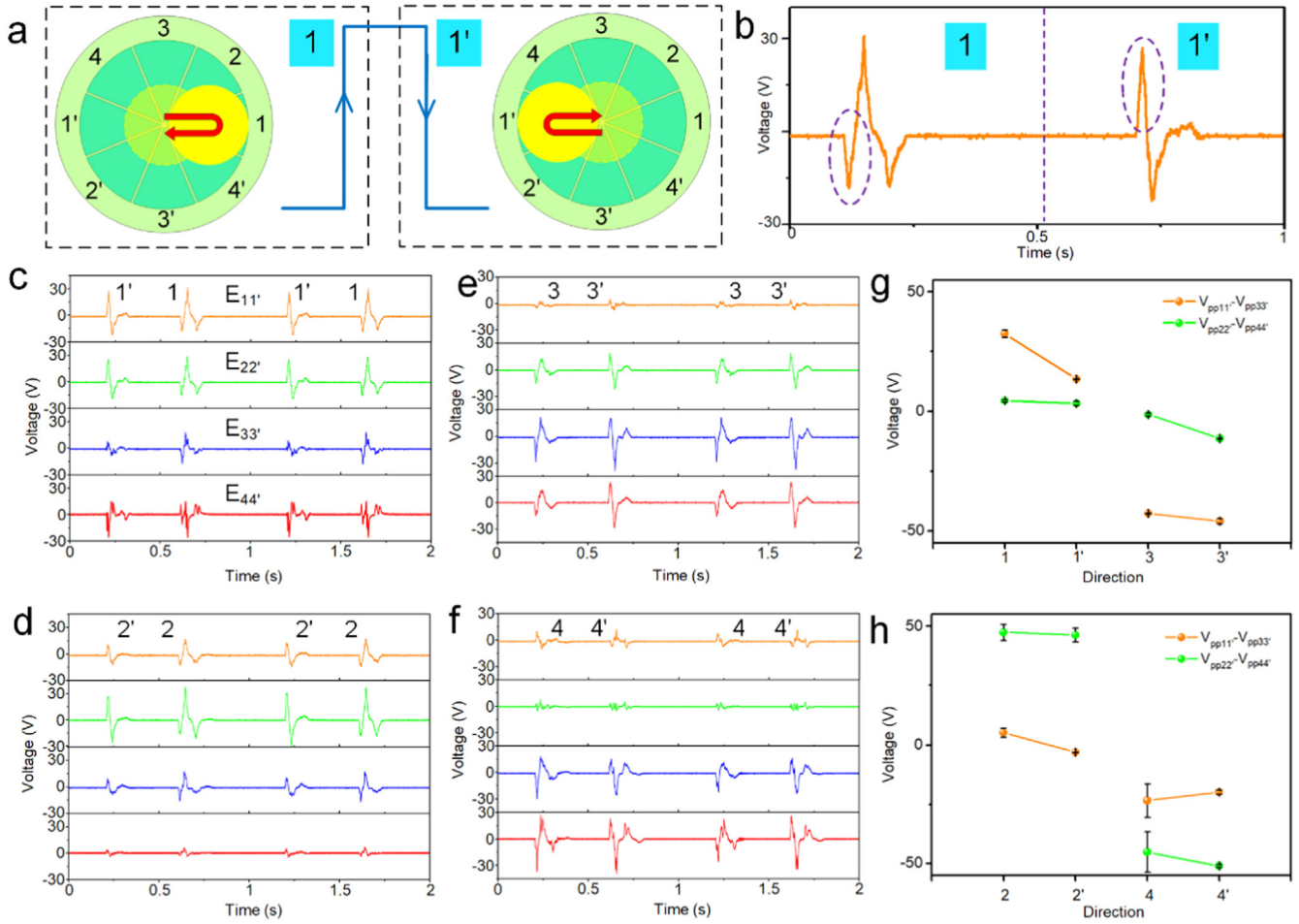

Fig. 5. Vibration direction sensing of TENG under pulse signal excitation. (a) Schematic diagram illustrating the motion of mass under a square signal. (b) The output signal generated by electrodes $E_{11'}$ when the device activated along direction of 11′. (c-f) The comparison of output signal among four electrode pairs when the excitation direction along 11′, 22′, 33′ and 44′, respectively. The difference value of peak-to-peak voltage between the two perpendicular electrode pairs for helping distinguish motion directions when the device moves along (g) 11′, 33′ and (h) 22′, 44′.

4.5 V with a long charging time. By combining the two parts, the hybrid charging provides both the abilities of fast charging speed and high charging level (7 V).

4.1. Vibration direction sensing under pulse excitation

On basis of the working principle that output is related to the overlap area between Aluminum film and electrode, the four pairs of electrodes can also distinguish low-frequency pulse vibration at eight directions by furtherly analyzing the output signals. For operation, the device is actuated under a square signal with frequency of 1 Hz and duty cycle of 40%. The eight-petal electrode is measured by the four probes of oscilloscope with electrode *E1*, *E2*, *E3* and *E4* connected to the test pin of the probe and electrode *E1′*, *E2′*, *E3′* and *E4′* connected to the corresponding ground terminal of the probe. As revealed in Fig. 5a, taking the excitation direction of 11′ for example, when at the rising edge of the excitation signal, the device moves to the direction 1 suddenly and the magnet will shift to electrode *E1* first. During this process, the positive triboelectric charges on the magnet will make the potential on the electrode *E1* increase, thus driving electrons flow from electrode *E1′* to *E1*. Therefore, a negative signal will be first tested on the channel 1 of oscilloscope, as shown in the front part of Fig. 5b. Then at the falling edge of the excitation signal, the device is dragged to the direction of 1′ suddenly and the magnet will shift to the electrode *E1*' first and then return to the center. Under this movement, the channel 1 of oscilloscope will first read a positive signal, as shown in the second part of Fig. 5b. Based on the signal relative values of the four electrode pairs and the sign bits, pulse movement for eight directions can be decided. Fig. 5c to f display the output voltages of the four pairs of electrode under the excitation of two sequential square signal along different directions. It is clear that the sign bits of the first peak in the output signal generated by the electrode pairs are quite different under various excitation directions.

In some practical vibration cases, the instability of vibration or the nonuniformly distributed triboelectric charges at Kapton surface may result in the output from the electrode pairs along the vibration direction being as large as that of the slant direction. In order to solve the problem, we propose a difference value method to help the judgement of the vibration direction by calculating the difference of peak-to-peak voltage between the orthogonal electrode pairs, that is '$V_{pp11'}$-$V_{pp33'}$'and '$V_{pp22'}$-$V_{pp44'}$', as shown in Fig. 5g, h. Form above analysis can be seen, the electrode along the moving direction has the largest output while the electrode perpendicular moving direction has the smallest output. When the device vibrates at the direction of 1 or 1′, the difference between $V_{pp11'}$ and $V_{pp33'}$ is a large positive value while that for the $V_{pp22'}$ and $V_{pp44'}$ is almost zero. When it comes to the direction of 3 and 3′, '$V_{pp11'}$-$V_{pp33'}$' will be a large negative value while '$V_{pp22'}$-$V_{pp44'}$' is almost zero. The properties are the same for the other situations. Detail analysis for the eight situations can be found in Table S1. Since the output perpendicular to the vibration direction tend to be the smallest and the outputs slant the direction are almost the same, combining the difference value method together with the maximum value method can

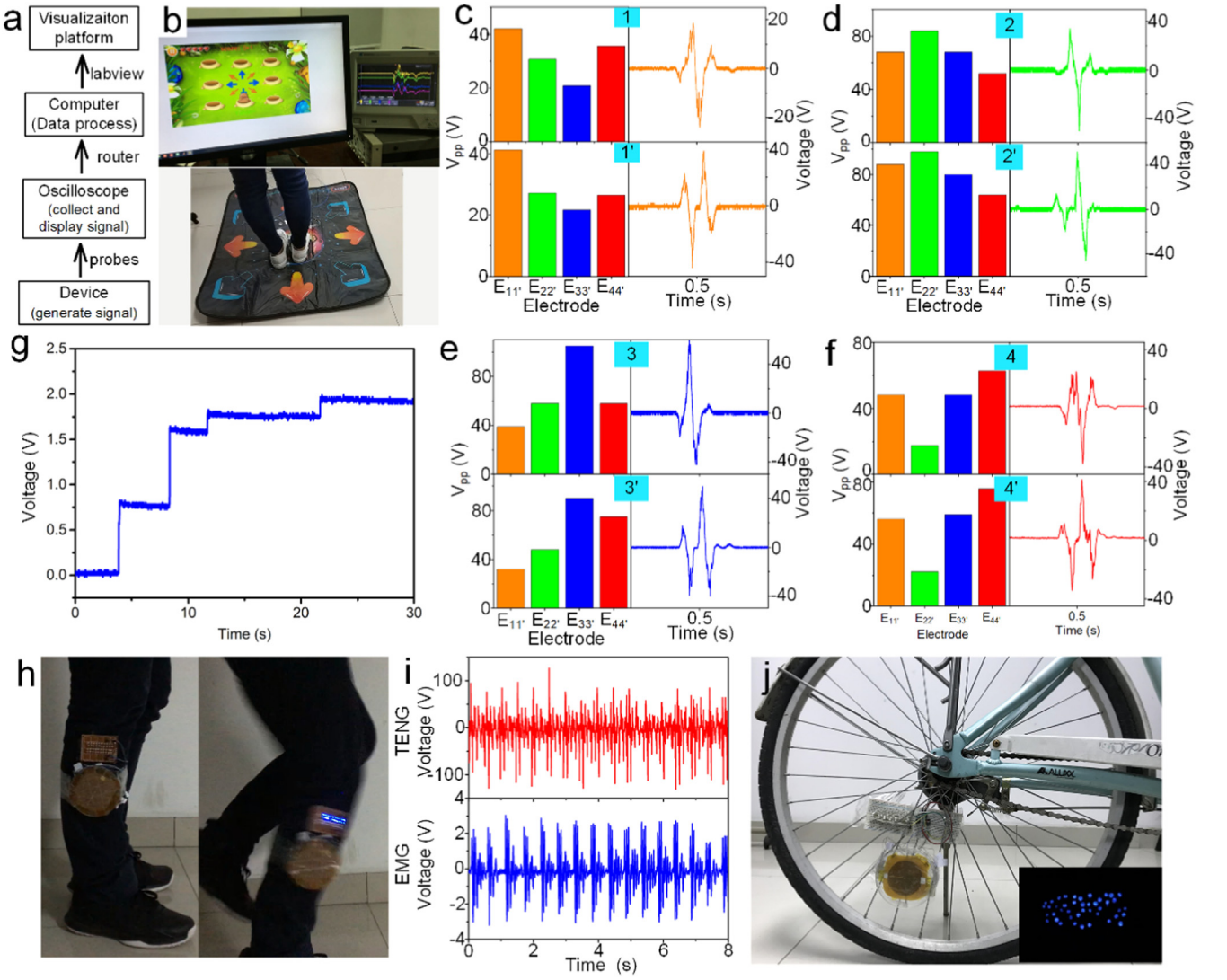

Fig. 6. Application demonstrations of the device as a self-powered motion sensor and an energy harvester. (a) System design flow of playing the "HitHamster" game by using the hybrid generator. (b) The enlarged view of the game visualization and device driving platform. (c-f) The comparison of output voltages generated by the TENG electrodes when the foot moves along the direction of 11′, 22′, 33′ and 44′, respectively. (h) Photograph of the device for harvesting energy of human running and lighting up LEDs. (i) The output voltages of the device during human running. (j) The photograph of the device mounted on a bicycle wheel for harvesting brake energy.

reduce judgement errors effectively.

4.2. Applications

The practicability of distinguishing vibration direction under periodical or pulse excitation enables the hybrid generator to detect body movement like swinging leg. As for application demonstration, we choose the spring with a wire diameter of 0.2 mm to obtain higher sensitivity. To prove the capability of the device as a self-powered vibration direction sensor, a "HitHamster" game is designed and implemented with the device as the human-machine interface. Fig. 6a shows the hardware system design of the game. In brief, the device is mounted on the front surface of the shoe for sensing the motion direction of foot. The signals generated from four TENG electrode pairs are collected and displayed by the oscilloscope through four probes. Simultaneously, the signal data is sent to the computer through a router and analyzed by the Labview software. After a series of data analysis using the method mentioned above, the motion direction can be determined and the action of the "hamster" on the computer screen can be controlled (see Supporting Information Video S1). Fig. 6b shows the enlarged view of game interface, acquired signals by the oscilloscope and the device driving platform. In the demonstration, a thinner spring can greatly decrease the natural frequency of the device, enabling the magnet to generate a large displacement under low-frequency body movement. The comparison of the output signals when the foot moving to different directions and the corresponding waveforms generated by the electrodes along the moving direction are presented in Fig. 6c to f. Since the device is placed horizontally on the foot with electrode *E3* towards the front, the motion of the magnet is similar to the situation under pulse vibration when the leg moves to arbitrary in-plane direction. It can be seen that the output properties are in accordance with the previous measurement and thus proving that the device is able to sense motion direction in practical applications. Since our device can generate both triboelectric and electromagnetic output at the same time, when the TENG part is used for sensing direction, the output of EMG can be stored in a capacitor for powering other electronics. As shown in Fig. 6g, the output of EMG under several times of leg motion is capable of charging the 20 μF capacitor to 2 V easily.

Supplementary material related to this article can be found online at http://dx.doi.org/10.1016/j.nanoen.2018.04.024.

Besides, the hybrid generator is capable of harvesting ambient vibration energy from arbitrary in-plane directions. To explore the capability of the device as a sustainable power source, the hybrid generator is mounted on a human leg to harvest the vibration energy from human running, as is shown in Fig. 6h. Under the excitation of human movement, 20 commercial LEDs in series and 20 LEDs in parallel were lit up by TENG and EMG, respectively. (see Supporting information Video S2). Fig. 6i shows the output voltages of the TENG and EMG under people running. During each step, the magnet vibrates up and down for several times, generating EMG output up to 3 V and TENG output up to 100 V. Furthermore, the device can be anchored on a bicycle wheel to harvest vibration energy when the bicycle jolt and act as a self-powered stoplight, as shown in Movie S3. Fig. 6j shows the LEDs lit up by the hybrid generator when braking, indicating that the device works as an effective random vibration energy harvester.

Supplementary material related to this article can be found online at http://dx.doi.org/10.1016/j.nanoen.2018.04.024.

5. Conclusions

In summary, we have demonstrated a hybrid generator based on the freestanding magnet that can be used for harvesting random low-frequency mechanical energy and detecting vibration direction. In this design, magnet, on one hand, is used as the vibration mass to work as a part of EMG. On the other hand, the magnet together with the Aluminum film adhered on it form a friction layer of TENG, thus hybridizing the TENG with EMG in a compact formation. What's more, the eight-petal electrode design of TENG enables the device to distinguish multiple in-plane vibration directions not only activated by periodical signal but also in the pulse form. As an energy harvester, the device is able to generate maximum power of 85.7 μW and 3.29 mW with one electrode pair of TENG and EMG coil, respectively. Based on the output characteristic of TENG and EMG, the hybrid device can charge a capacitor to a high voltage with a rapid charging efficiency. Several applications of harvesting energy have been demonstrated including the mechanical vibration from human running and braking energy on the bicycle wheel, which indicates its tremendous potential in building self-powered systems by harvesting ambient vibrational energy. Furthermore, a motion sensing game is designed to prove the capability of the device as a self-powered vibration direction sensor. The superior vibration sensing capacity enables the hybrid generator to detect many features of vibration such as direction and frequency, showing its great potential in the field of self-powered sensing systems including alarms, environmental/infrastructure monitoring and motion recognition.

Acknowledgements

This work is supported by the National Key Research and Development Program of China (2016YFA0202701), National Natural Science Foundation of China (Grant No. 61674004 and 91323304), and the Beijing Science & Technology Project (Grant No. D151100003315003).

Appendix A. Supporting information

Supplementary data associated with this article can be found in the online version at http://dx.doi.org/10.1016/j.nanoen.2018.04.024.

References

[1] J. Chen, G. Zhu, W. Yang, Q. Jing, P. Bai, Y. Yang, T.C. Hou, Z.L. Wang, Adv. Mater. 25 (2013) 6094–6099.
[2] Y. Hu, J. Yang, Q. Jing, S. Niu, W. Wu, Z.L. Wang, ACS Nano 7 (2013) 10424–10432.
[3] D.Y. Kim, H.S. Kim, D.S. Kong, M. Choi, H.B. Kim, J.-H. Lee, G. Murillo, M. Lee, S.S. Kim, J.H. Jung, Nano Energy 45 (2018) 247–254.
[4] Y. Bian, T. Jiang, T. Xiao, W. Gong, X. Cao, Z. Wang, Z.L. Wang, Adv. Mater. Technol. 3 (2018) 1700317.
[5] R. Liu, X. Kuang, J. Deng, Y.C. Wang, A.C. Wang, W. Ding, Y.C. Lai, J. Chen, P. Wang, Z. Lin, Adv. Mater. 30 (2018) 1705195.
[6] S. Meninger, J.O. Mur-Miranda, R. Amirtharajah, A. Chandrakasan, J.H. Lang, IEEE Trans. Very Large Scale Integr. (VLSI) Syst. 9 (2001) 64–76.
[7] S. Roundy, P.K. Wright, J. Rabaey, Comput. Commun. 26 (2003) 1131–1144.
[8] C. Williams, R.B. Yates, Sens. Actuators A: Phys. 52 (1996) 8–11.
[9] R. Amirtharajah, A.P. Chandrakasan, IEEE J. Solid-State Circuits 33 (1998) 687–695.
[10] Z.L. Wang, J. Song, Science 312 (2006) 242–246.
[11] G. Zhu, A.C. Wang, Y. Liu, Y. Zhou, Z.L. Wang, Nano Lett. 12 (2012) 3086–3090.
[12] Y. Hu, Y. Zhang, C. Xu, L. Lin, R.L. Snyder, Z.L. Wang, Nano Lett. 11 (2011) 2572–2577.
[13] S. Roundy, E.S. Leland, J. Baker, E. Carleton, E. Reilly, E. Lai, B. Otis, J.M. Rabaey, P.K. Wright, V. Sundararajan, IEEE Pervasive Comput. 4 (2005) 28–36.
[14] Z.L. Wang, ACS Nano 7 (2013) 9533–9557.
[15] X.-S. Zhang, M.-D. Han, R.-X. Wang, F.-Y. Zhu, Z.-H. Li, W. Wang, H.-X. Zhang, Nano Lett. 13 (2013) 1168–1172.
[16] B. Meng, W. Tang, Z.-h. Too, X. Zhang, M. Han, W. Liu, H. Zhang, Energy Environ. Sci. 6 (2013) 3235–3240.
[17] M. Han, X.-S. Zhang, B. Meng, W. Liu, W. Tang, X. Sun, W. Wang, H. Zhang, ACS Nano 7 (2013) 8554–8560.
[18] K. Dong, J. Deng, Y. Zi, Y.C. Wang, C. Xu, H. Zou, W. Ding, Y. Dai, B. Gu, B. Sun, Adv. Mater. 29 (2017) 1702648.
[19] S.W. Chen, X. Cao, N. Wang, L. Ma, H.R. Zhu, M. Willander, Y. Jie, Z.L. Wang, Adv. Energy Mater. 7 (2017) 1601255.
[20] K. Parida, V. Kumar, W. Jiangxin, V. Bhavanasi, R. Bendi, P.S. Lee, Adv. Mater. 29 (2017) 1702181.
[21] J. Yang, J. Chen, Y. Yang, H. Zhang, W. Yang, P. Bai, Y. Su, Z.L. Wang, Adv. Energy Mater. 4 (2014) 1301322.
[22] H. Askari, Z. Saadatnia, E. Asadi, A. Khajepour, M.B. Khamesee, J. Zu, Nano Energy 45 (2018) 319–329.
[23] K. Zhang, X. Wang, Y. Yang, Z.L. Wang, ACS Nano 9 (2015) 3521–3529.
[24] X. Wang, Z. Wen, H. Guo, C. Wu, X. He, L. Lin, X. Cao, Z.L. Wang, ACS Nano 10 (2016) 11369–11376.
[25] H. Guo, Z. Wen, Y. Zi, M.H. Yeh, J. Wang, L. Zhu, C. Hu, Z.L. Wang, Adv. Energy Mater. 6 (2016) 1501593.
[26] Y. Hu, J. Yang, S. Niu, W. Wu, Z.L. Wang, ACS Nano 8 (2014) 7442–7450.
[27] L.C. Rome, L. Flynn, E.M. Goldman, T.D. Yoo, Science 309 (2005) 1725–1728.
[28] J.M. Donelan, Q. Li, V. Naing, J. Hoffer, D. Weber, A.D. Kuo, Science 319 (2008) 807–810.
[29] S. Wang, S. Niu, J. Yang, L. Lin, Z.L. Wang, ACS Nano 8 (2014) 12004–12013.
[30] H. Zhang, Y. Yang, Y. Su, J. Chen, K. Adams, S. Lee, C. Hu, Z.L. Wang, Adv. Funct. Mater. 24 (2014) 1401–1407.
[31] M. Han, X.-S. Zhang, X. Sun, B. Meng, W. Liu, H. Zhang, Sci. Rep. 4 (2014) 4811.
[32] Y. Wu, Q. Jing, J. Chen, P. Bai, J. Bai, G. Zhu, Y. Su, Z.L. Wang, Adv. Funct. Mater. 25 (2015) 2166–2174.
[33] B. Zhang, L. Zhang, W. Deng, L. Jin, F. Chun, H. Pan, B. Gu, H. Zhang, Z. Lv, W. Yang, ACS Nano 11 (2017) 7440–7446.
[34] Q. Shi, H. Wu, H. Wang, H. Wu, C. Lee, Adv. Energy Mater. 7 (2017) 1701300.
[35] X. Wang, H. Zhang, L. Dong, X. Han, W. Du, J. Zhai, C. Pan, Z.L. Wang, Adv. Mater. 28 (2016) 2896–2903.
[36] X. Pu, M. Liu, X. Chen, J. Sun, C. Du, Y. Zhang, J. Zhai, W. Hu, Z.L. Wang, Sci. Adv. 3 (2017) e1700015.
[37] Q. Shi, H. Wang, H. Wu, C. Lee, Nano Energy 40 (2017) 203–213.
[38] H. Yu, X. He, W. Ding, Y. Hu, D. Yang, S. Lu, C. Wu, H. Zou, R. Liu, C. Lu, Adv. Energy Mater. 7 (2017) 700565.
[39] X. Chen, Y. Song, Z. Su, H. Chen, X. Cheng, J. Zhang, M. Han, H. Zhang, Nano Energy 38 (2017) 43–50.
[40] Z. Lin, J. Chen, X. Li, Z. Zhou, K. Meng, W. Wei, J. Yang, Z.L. Wang, ACS Nano 11 (2017) 8830–8837.
[41] M. Shi, H. Wu, J. Zhang, M. Han, B. Meng, H. Zhang, Nano Energy 32 (2017) 479–487.
[42] S. Niu, Y. Liu, X. Chen, S. Wang, Y.S. Zhou, L. Lin, Y. Xie, Z.L. Wang, Nano Energy 12 (2015) 760–774.
[43] R. Cao, T. Zhou, B. Wang, Y. Yin, Z. Yuan, C. Li, Z.L. Wang, ACS Nano 11 (2017) 8370–8378.